Chemical Science

ROYAL SOCIETY OF CHEMISTRY

EDGE ARTICLE

View Article Online
View Journal | View Issue

Cite this: *Chem. Sci.*, 2021, **12**, 5177

All publication charges for this article have been paid for by the Royal Society of Chemistry

Received 5th January 2021
Accepted 16th February 2021

DOI: 10.1039/d1sc00060h

rsc.li/chemical-science

Coupling molecular rigidity and flexibility on fused backbones for NIR-II photothermal conversion†

Yonglin He, ‡[a] Hailiang Liao,‡[b] Shanzhi Lyu,[a] Xiao-Qi Xu,[a] Zhengke Li,[b] Iain McCulloch,[c] Wan Yue *[b] and Yapei Wang *[a]

Great attention is being increasingly paid to photothermal conversion in the near-infrared (NIR)-II window (1000–1350 nm), where deeper tissue penetration is favored. To date, only a limited number of organic photothermal polymers and relevant theory have been exploited to direct the molecular design of polymers with highly efficient photothermal conversion, specifically in the NIR-II window. This work proposes a fused backbone structure locked *via* an intramolecular hydrogen bonding interaction and double bond, which favors molecular planarity and rigidity in the ground state and molecular flexibility in the excited state. Following this proposal, a particular class of NIR-II photothermal polymers are prepared. Their remarkable photothermal conversion efficiency is in good agreement with our strategy of coupling polymeric rigidity and flexibility, which accounts for the improved light absorption on going from the ground state to the excited state and nonradiative emission on going from the excited state to the ground state. It is envisioned that such a concept of coupling polymeric rigidity and flexibility will offer great inspiration for developing NIR-II photothermal polymers with the use of other chromophores.

Introduction

In terms of its low absorption by hemoglobin and water in tissue environments, near-infrared light (NIR) between 1000 and 1350 nm, or NIR-II for short, is generally regarded as a more biological transparent window than other wavelengths.[1] Besides this, human tissues also exhibit a higher tolerance to NIR-II light in contrast to light with a shorter wavelength. These attractive advantages essentially satisfy the need for optically non-invasive diagnosis and treatment in deep tissues.[2–7] The past few years have witnessed an explosive development in photothermal conversion, which is considered to be an innovative way to use NIR-II light with high quantum efficiency.[4,8,9] Referring to the principles of photothermal conversion, photothermal materials with the ability to convert light energy to thermal energy are critically important. Benefiting from their easy modification, good biocompatibility, and potential biodegradability, organic photothermal materials are attracting great interest in addition to the investigation of inorganic nanoparticles.[10–16] However, only a limited number of organic NIR-II photothermal materials have been exploited so far. The successful examples have mostly been formulated using conjugated polymers, which possess a low bandgap to meet the light absorption in the NIR window. Rarely has attention been paid to theoretical ideas for directing the molecular design of polymers that prefer to absorb NIR-II light, and also exhibit highly efficient photothermal conversion.[2,17–19]

In principle, the photothermal conversion process of NIR-II molecules can be described using eqn (1),

$$Q = I_0 \times (1 - 10^{A}) \times \phi_{IC} \quad (1)$$

where Q is the heating power based on the photothermal conversion and I_0 is the light intensity. The photothermal conversion consists of two processes, including light absorption (A) and non-irradiative emission. Regardless of the concentration and the optical path, the extinction coefficient (ε) of the molecules is an intrinsic factor that affects the light absorption, which is closely related to the electronic state of the molecule. The efficiency of internal conversion (ϕ_{IC}) is a crucial factor by which to determine the non-irradiative emission, which is generally affected by the vibrational state of the molecule. Nevertheless, the light absorbing process and internal conversion process are competitive in terms of their molecular structure requirements. In order to ensure light absorption in the NIR-II window, the energy gap between the ground and excited states should be below 1.24 eV, which relies on molecular planarity and rigidity,

[a]*Department of Chemistry, Renmin University of China, Beijing 100872, China. E-mail: yapeiwang@ruc.edu.cn*

[b]*State Key Laboratory of Optoelectronic Materials and Technologies, Key Laboratory for Polymeric Composite and Functional Materials of Ministry of Education, Guangzhou Key Laboratory of Flexible Electronic Materials and Wearable Devices, School of Materials Science and Engineering, Sun Yat-Sen University, Guangzhou 510275, China. E-mail: yuew5@mail.sysu.edu.cn*

[c]*Department of Chemistry, University of Oxford, 12 Mansfield Road, Oxford OX1 3TA, UK*

† Electronic supplementary information (ESI) available. See DOI: 10.1039/d1sc00060h

‡ These authors contributed equally to this work.

with better electron delocalization (Fig. 1a).[20–23] However, the dissipation of excited states *via* internal conversion is more favored in the case of molecules with less rigidity, for example, with rotatable or vibrational bonds (Fig. 1b).[24] Therefore, organic NIR-II photothermal materials with better photothermal conversion efficiency may be exploited through the choice of coupling the structural rigidity with flexibility.

Following the strategy of coupling rigidity and flexibility, we successfully developed a type of polymers that have low energy gaps and high photothermal conversion efficiency (Fig. 1c). As illustrated in Fig. 1d–f, the three polymers are all composed of a fused backbone structure in which the free rotation of molecular fragments is extremely restricted by the interconnected double bonds and intramolecular hydrogen bonding interaction, ensuring higher molecular planarity and electron delocalization along the polymer chain. However, the hydrogen bonding cannot fully lock the molecular skeleton and the length of the double bond becomes longer, with a certain degree of molecular torsion occurring in the excited state. This unique characteristic is beneficial for internal conversion by means of vibration relaxation.

Results and discussion

Polymer synthesis

Three polymers with different heteroatoms were synthesized *via* an acid-catalyzed aldol polymerization from different precursor monomers (Schemes 1, S1–S3 and Fig. S1–S5†), including naphthalene bis-isatin,[25,26] benzenedifurandione,[27] and benzodithiophene-dione.[28] As measured by high-temperature gel permeation chromatography (GPC), the molecular weights (M_n) of **Y1**, **Y2**, and **Y3** are 67.3, 25.2, and 21.1 kDa, respectively. These polymers are all soluble in halogenated solvents, for example, chloroform, chlorobenzene (CB), and *o*-dichlorobenzene (DCB). The decomposition temperatures with a 5.0% weight loss are 377 °C for **Y1**, 345 °C for **Y2**, and 376 °C for **Y3**, according to the thermogravimetric analysis (TGA) (see Fig. S6–S8†). The lower decomposition temperature of **Y2** might be attributed to the low stability of the thioester groups in the structure of 3,7-bis((*E*)-2-oxoindolin-3-ylidene)-3,7-dihydrobenzo[1,2-b:4,5-b′]dithiophene-2,6-dione (IBDT).[28,29] In practice, these decomposition temperatures are high enough to ensure desirable thermal stability in the particular cases of biologically photothermal applications.

Light absorption and electron excitation

The light absorption properties of the three polymers were evaluated within a range from 400 to 1600 nm (Fig. S9 and S10†). As shown in Fig. 2 and S9,† the vis-NIR absorption spectra of **Y1**, **Y2**, and **Y3** dissolved in chlorobenzene were investigated upon changing the polymer concentration as well as the temperature. The three polymers all exhibit remarkable absorption in the NIR-II window. As theoretically predicted in

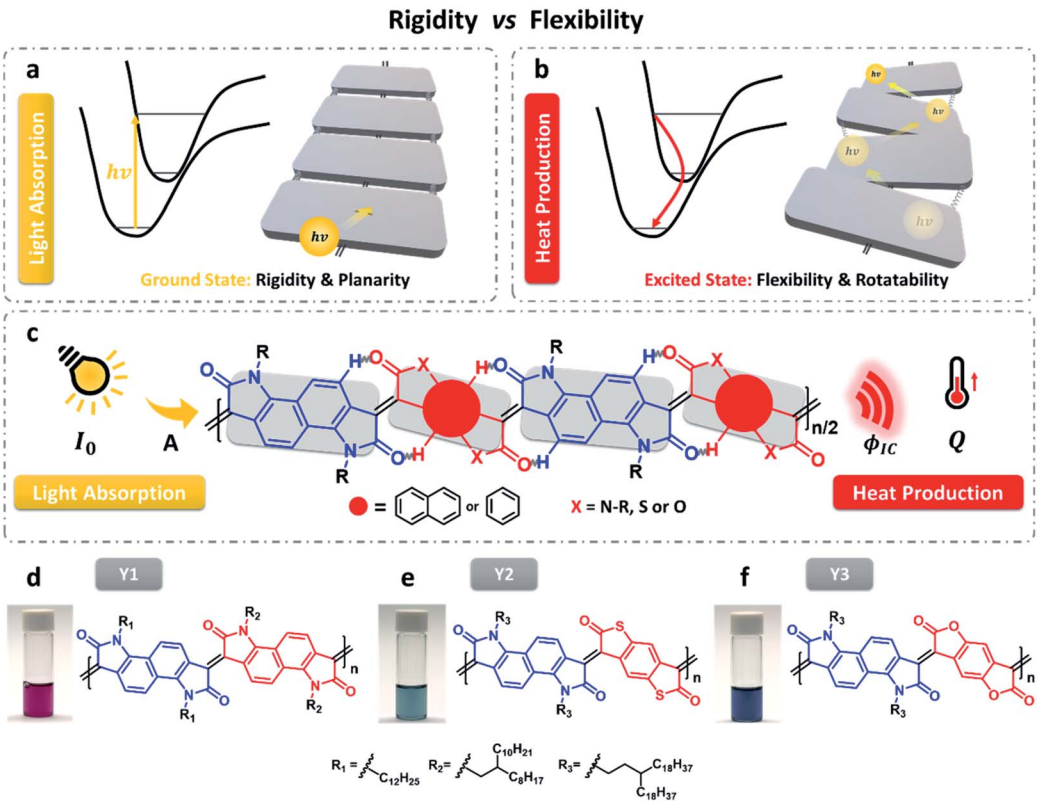

Fig. 1 Ideal molecular design of organic NIR-II photothermal materials, which require (a) molecular rigidity and planarity in the ground state and (b) molecular flexibility and rotatability in the excited state. (c) Design of NIR-II photothermal polymers and schematic illustration of the related photothermal process. Images of the three polymer solutions (50 μg ml^{-1} in chlorobenzene) and their specific molecular structures, from left to right, (d) **Y1**, (e) **Y2**, and (f) **Y3**, respectively.

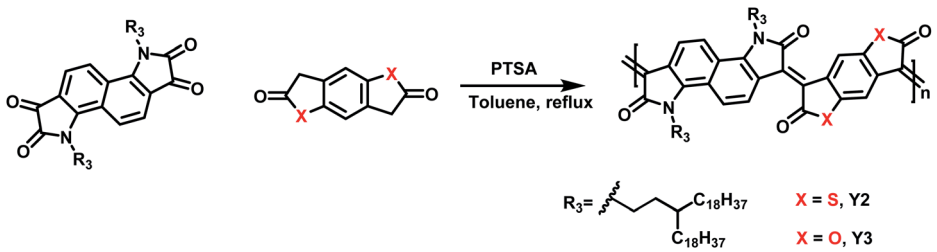

Scheme 1 Synthetic route for the Y2 and Y3 polymers.

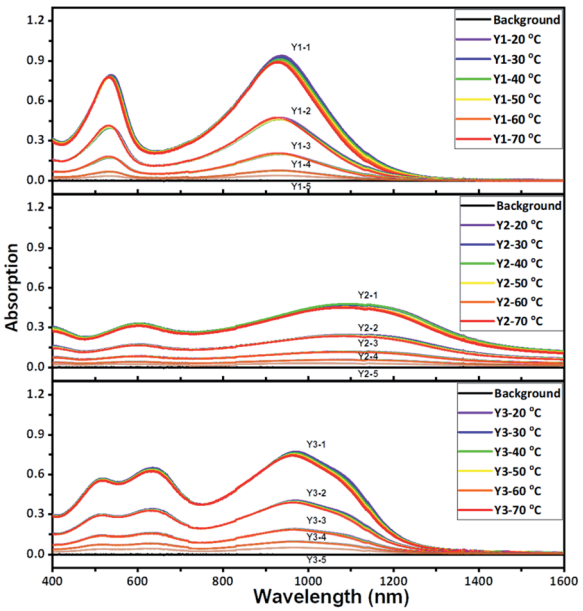

Fig. 2 Absorption spectra of Y1, Y2, and Y3 (from top to bottom) in chlorobenzene solutions. The absorption curves of each polymer at different concentrations and temperatures are provided in the boxes, respectively. The curves of the same color, from top to bottom for each polymer, represent the absorption spectra of samples with a concentration of 400 μg ml^{-1} (Y1-1, Y2-1, and Y3-1), 200 μg ml^{-1} (Y1-2, Y2-2, and Y3-2), 100 μg ml^{-1} (Y1-3, Y2-3, and Y3-3), 50 μg ml^{-1} (Y1-4, Y2-4, and Y3-4), and 25 μg ml^{-1} (Y1-5, Y2-5, and Y3-5). The black curve is the background absorption of the pure chlorobenzene solution. The different colors of the curves represent different temperatures, ranging from 20 to 70 °C at intervals of 10 °C.

Fig. S11–S13,† the experimental spectra closely overlap with the calculated spectra of the dimers and trimers, suggesting that the effective conjugation lengths of these polymers are likely to fall between two and three repeating units. The ion potentials (IPs) of **Y1**, **Y2**, and **Y3**, as measured by X-ray photoelectron spectroscopy (XPS) in air, are 5.20, 5.36, and 5.71 eV, which are basically consistent with the estimation of the highest occupied molecular orbital (HOMO) (Fig. S14†). Referring to the theoretical light absorption spectra of the trimers (Fig. S15†), the three polymers are more likely to accept aromatic configuration rather than quinoid configuration.[30] It is worth noting that the temperature has little influence on the absorption spectra of the three polymers at the given polymer concentrations. There is no blue shift when the temperature is increased, suggesting that the light absorption in the NIR-II window is not a result of *J*-aggregation.[31,32] The linear correlation of the absorbance with the polymer concentration, which is entirely consistent with the Lambert–Beer law (Fig. S16†), also supports the assumption of negligible molecular aggregation in chlorobenzene.

The maximum absorption peaks (λ_P) of **Y1**, **Y2**, and **Y3** are 937, 1107, and 970 nm, respectively, obeying an order of $\lambda_{P\text{-}Y2} > \lambda_{P\text{-}Y3} > \lambda_{P\text{-}Y1}$. Whereas, the order of the molar extinction coefficient (ε_m) is the reverse, $\varepsilon_{m\text{-}Y1} > \varepsilon_{m\text{-}Y3} > \varepsilon_{m\text{-}Y2}$. Both the maximum absorption order and molar extinction order are also supported by theoretical calculations (Fig. S12 and S13†). In principle, λ_P and ε_m rely on the molecular rigidity and coplanar properties. In general, better coplanar property leads to greater delocalization of the electrons, thereby enabling intense light absorption at a longer wavelength.[33,34] To decide if the order of λ_P and ε_m are influenced by the coplanar properties, the trimers of the three polymers were optimized in terms of their configurations *via* density functional theory (DFT) calculations (Fig. S21†). These trimers possess pronounced coplanarity, except for the dione groups, where small torsion is observed, which probably accounts for the indistinct molecular aggregation. The dihedral angle of the three polymers is in the order of $\theta_{S0\text{-}Y3} < \theta_{S0\text{-}Y1} < \theta_{S0\text{-}Y2}$, unlike the orders of λ_P or ε_m. In this regard, the molecular coplanarity alone could not be used to explain the absorption difference of the three polymers directly.

In principle, the distinct light absorption is relevant to electron transition from the ground state to the excited state under light irradiation. So, understanding the process of electron transition is favorable for explaining the order of the absorption wavelength as well as the molar extinction coefficient. As illustrated in Fig. 3a, the electron excitation generally follows the rule of Franck–Condon transitions from S_0V_0 to S_1V_m, in which the energy gap corresponds to the absorption wavelength (λ_P). Because an excitation of electron transition mostly involves a number of molecular orbitals, the total electron cloud either in the ground state or the excited state is calculated by integrating all the molecular orbitals involved in the transition process based on hole–electron analysis.[35] As summarized in Fig. 3c, the electron cloud in the ground state is originally distributed on the bonding region within the benzene ring, and then moves to individual atoms in the excited state. Similar electron cloud changes were also observed for polymers with different effective conjugation lengths (Fig. 3c and S17–S20†). This electron transition can be classified as a π–π* transition. Besides this, a distinct donor–acceptor electron

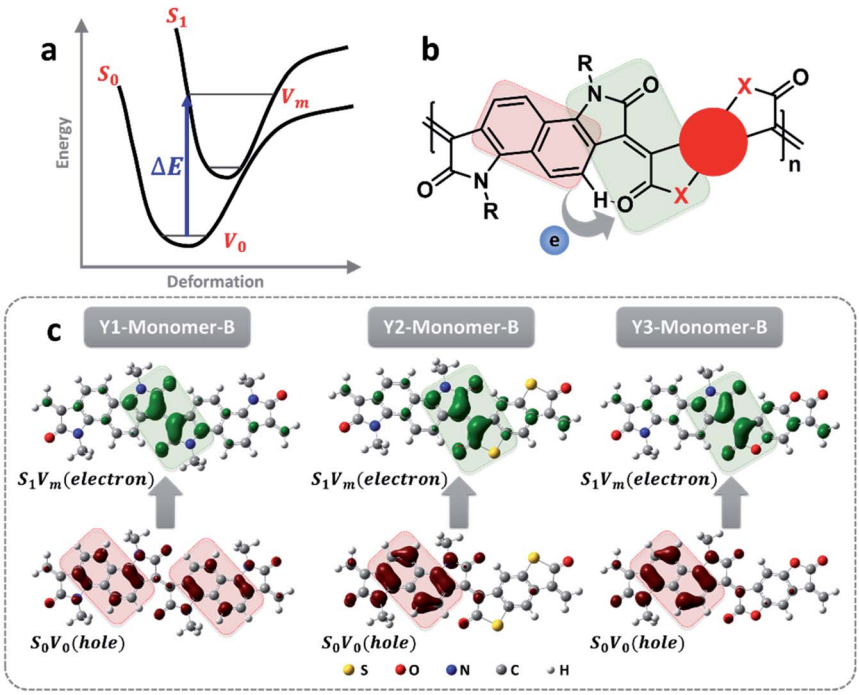

Fig. 3 Structure–property analysis of light absorption. (a) Schematic energy diagram of the transition corresponding to the maximum absorption peak. (b) Schematic illustration of electron changes in the transition, in which the structure of the light red box is where the hole of the ground state is, and that of the light green box is where the electron excited state is. During the transition, the electron goes from the light red box to the light green box. The detailed changes are provided in (c), and the dark red and green parts indicate the hole and electron clouds of all of the molecular orbitals in the ground and excited states related to the transition. The isovalue is 0.002.

transfer process from the donor segment, naphthalene, to the electron-deficient dione groups was also observed (Fig. 3b). This D–A electron transfer process reduces the energy gap, leading to a significant redshift in the absorption wavelength.[36] The larger conjugation length is another factor that accounts for the absorption at a longer wavelength (Fig. S11–S13†).

Regardless of the influence of the dihedral angles within a conjugated repeating unit, the main structural difference among the three polymers lies in the heteroatoms near to the carbonyl group, referring to N, S, and O for **Y1**, **Y2**, and **Y3**, respectively. These three atoms all offer a positive conjugated effect and act as electron donors in the conjugated system. Concretely, the atomic radius of N is closer to C than O, and the π bonds between C and N, O are composed of their 2p orbitals. S possesses a larger radius than C, and its 3p orbitals take part in the formation of π bonds. The contribution of three atoms to the conjugation effect follows the order of N > O > S. As for the molecular structures in this work, the less conjugated the heteroatom is, the more electron deficient the dione group, corresponding to a lower lowest unoccupied molecular orbital (LUMO) energy level, namely $LUMO_{Y1} < LUMO_{Y3} < LUMO_{Y2}$ (Fig. S14†). In terms of the close HOMOs due to similar donor segments, a lower LUMO energy level corresponds to a narrower energy bandgap, which thus explains the order of $\lambda_{P\text{-}Y2} > \lambda_{P\text{-}Y3} > \lambda_{P\text{-}Y1}$.

The different extinction coefficients of the three polymers are also related to the factors of the donor–acceptor (D–A) structure and conjugation effect. Theoretically, the extinction coefficient (ε) is proportional to the overlap integral of the electron wave functions of the ground state φ_{S_0} and the excited state φ_{S_1}, which can be expressed using eqn (2),

$$\varepsilon \propto \langle \varphi_{S_0} | \mu | \varphi_{S_1} \rangle^2 \quad (2)$$

where μ is the electron transition dipole moment. The D–A and conjugation effects have opposite influences on the overlap of the electron wave functions. Improving the D–A effect generally gives rise to a lower extinction coefficient as a result of there being less overlap between the electron clouds of the ground and excited states. On the contrary, prolonging the conjugation length leads to a higher extinction coefficient owing to the greater degree of the electron transition. In comparison, **Y2** has the strongest D–A effect because its dione groups are the most electron deficient, while **Y1** has the weakest DA effect. Meanwhile, **Y1** consists of more naphthalene segments, which accounts for its longer conjugation length (Fig. S17–S20†). Therefore, **Y1** has a higher extinction coefficient than the other two polymers. Incidentally, it should be noted that molecular planarity is essential for the DA or conjugation effects, although it is not responsible for the absorption difference among these three polymers.

Photothermal conversion and vibrational relaxation

The photothermal conversion properties of these three polymers were investigated after the experimental and theoretical evaluation of their light absorption properties. As shown in

Fig. 4, the three polymers dissolved in chlorobenzene with the same absorbance *via* adjusting polymer concentrations were compared and subjected to NIR-II light irradiation under different power densities. As recorded using an infrared (IR) camera, the temperature of each polymer solution rapidly rises under NIR light irradiation. The temperature difference compared to room temperature is positively related to the light power (Fig. S22†). For example, at a light power of 0.9 W, the temperature increases by 20.8 °C relative to room temperature for the **Y3** solution, and 15.1 and 16.6 °C for the **Y1** and **Y2** solutions, respectively. Notably, the control group consisting of only chlorobenzene exhibits a negligible response to NIR light irradiation, as its temperature only increases by 0.5 °C, confirming that it is the polymers rather than chlorobenzene that are responsible for the photothermal effect. Reversible cycles of on–off NIR light irradiation under different light powers reveal that the three polymers possess excellent photostability (Fig. 4b). The completely reproducible temperature changes suggest that the photothermal effect results from a photophysical process rather than chemical reactions. The photothermal energy can be specified by summing the increased heat in polymer solution and thermal dissipation, as shown in eqn (3):

$$Q = \sum m_i C_{pi} \frac{dT}{dt} + hA(T - T_0) \quad (3)$$

where the mass and specific heat capacity of the heated material in the process are m_i and C_{pi}, respectively. T_0 is the room temperature, which is 20 °C. T is the temperature of the system after NIR light irradiation for a period of time (t), and Q is the generation rate of photothermal heat. h and A are the thermal conductivity and heat dissipation area, respectively. The time-dependent temperature change is in full agreement with this equation, with an R-squared value of over 0.99, indicating that the equation is highly effective in evaluating the photothermal production. According to the derived generation rate of photothermal heat, the photothermal efficiencies of the **Y1**, **Y2**, and **Y3** polymer solutions under 0.5 W light irradiation are 67.9%, 69.5%, and 76.5%, respectively.

The photothermal effect is a result of relaxation from the excited to ground state. The pathways of intersystem crossing and fluorescent emission were ruled out in terms of the absence of singlet oxygen (Fig. S23†) and the unobserved fluorescence signal within the range of 1100–1800 nm under the excitation of a 1064 nm laser (Fig. S24†). So, the internal conversion is proposed to account for the electron relaxation along with non-irradiative emission in the form of thermal heat. As illustrated in Fig. 5a, the internal conversion process generally involves two steps, from the high vibrational energy level S_1V_m to the lowest vibrational energy level S_1V_0 of the excited state, and then from S_1V_0 to the ground state S_0V_0. The internal conversion rate generally depends on the second step as the first step is much faster.[14] The transformation of the molecular conformation between the ground and excited states is crucial to the internal conversion because it is closely related to the molecular vibrational energy level. As labeled in Fig. 5b, a dihedral angle, denoted as θ, is a representative parameter used to illustrate the primary conformation change between the ground and excited states. This assumption was confirmed using DFT calculations, as shown in Fig. 5d. The dihedral angles of the trimers of the three polymers decrease to a similar extent when they evolve from S_1V_0 to S_0V_0, in the order of **Y2** > **Y1** > **Y3**. In principle, the dihedral angle is a balanced result of two factors; one is the spatial repulsion of the molecular segments as bridged by the double bond, and the other is the hydrogen bond of the carbonyl group with the hydrogen atom on the neighboring benzene.

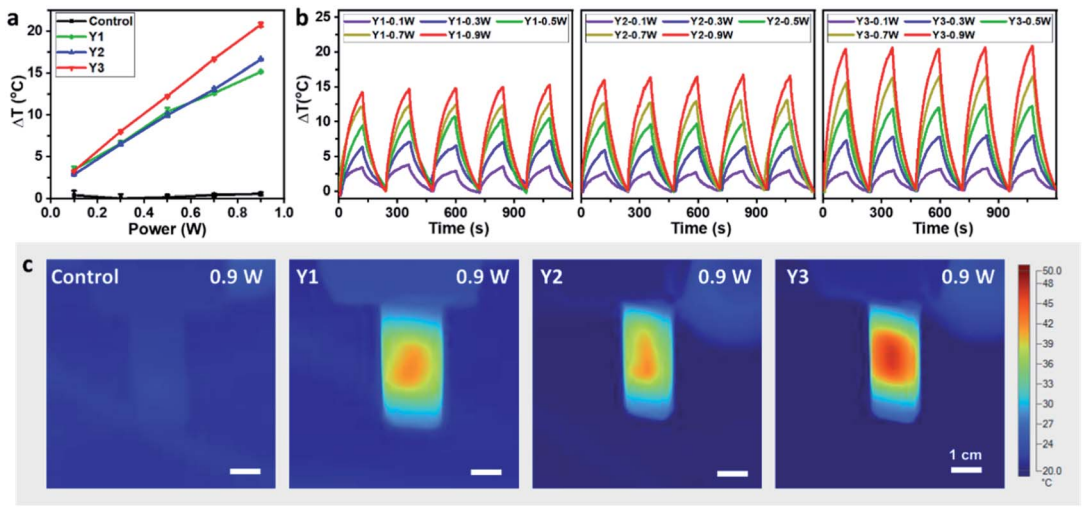

Fig. 4 Photothermal performance of the NIR-II photothermal polymers. (a) Temperature changes of their solutions irradiated using different light powers for 2 min, in which the control group is pure chlorobenzene. The wavelength of the laser is 1064 nm, and the absorbance of the polymer solutions is around 0.5, with an optical path length of 0.1 mm. (b) The on–off curve of the polymer solution irradiated using a 1064 nm laser of different power, and ΔT is the difference between the average temperature of the irradiated area and the room temperature (20 °C). (c) Temperature distributions of the polymer solution irradiated by a 0.9 W laser for 2 min.

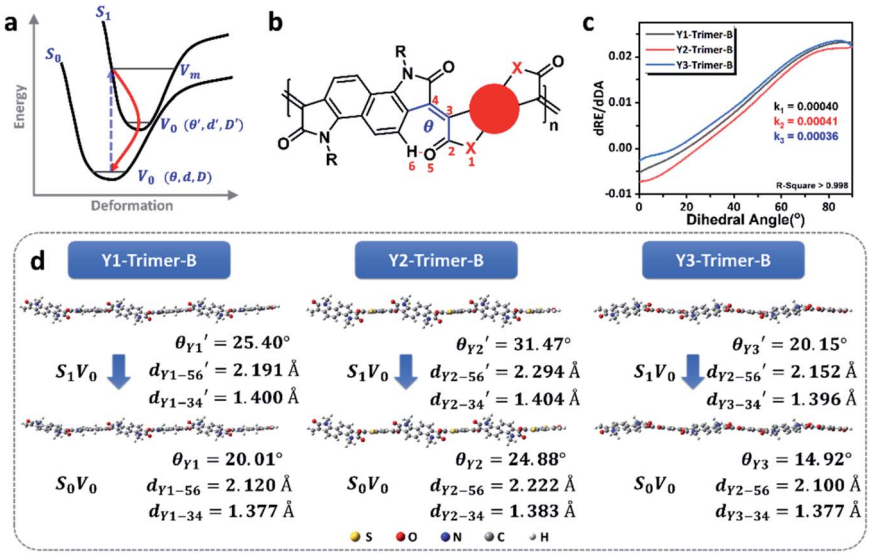

Fig. 5 Molecular vibration analysis of the NIR-II photothermal polymers. (a) Schematic diagram of the photothermal polymers from the excited state to the ground state *via* internal conversion. (b) Parameters included in the molecular vibration. The red numbers are used to specify atoms involved in the theoretical calculation. (c) Differential curve from the relative energy–dihedral angle curve. The intersection of the curve and the line dRE/dDA = 0 is the lowest energy point, and the corresponding relative energy is 0 eV. *k* is the slope of the linear variation region of the above curve from the intersection point to the largest dihedral angle. k_1, k_2, and k_3 correspond to the slopes of the curves of the **Y1**-trimer-B, **Y2**-trimer-B and **Y3**-trimer-B, respectively. (d) The dihedral angles and the corresponding hydrogen and double bond lengths of the three trimers in their optimal conformations in the ground and excited states.

To further understand the photothermal process, the Laplacian bond orders (*O*) of the double bonds,[37] the bond length (*d*), and atomic partial charges (*Q*) derived using the restrained electrostatic potential (RESP) approach in S_1V_0 (with a prime symbol) and S_0V_0 (without a prime symbol) were calculated (Fig. 5, Tables 1 and S1†). As shown in Fig. 5d, the length of the double bonds is longer than that of ethylene (1.339 Å) but indeed shorter than the carbon–carbon single bond of ethane (1.535 Å). This order is also applicable to the Laplacian bond orders of double bonds (Table 1). The weaker double bonds allow a certain degree of molecular distortion and are beneficial to the vibrational relaxation. It should be noted that these double bonds become even weaker in the excited states, which may be caused by the increase in the electron cloud on the two carbon atoms. Besides this, the hydrogen bonds in these polymers are assigned as being moderate in strength according to their length,[38] of which the interaction is generally electrostatic and their strength should be proportional to the electrostatic potential energy, namely $\frac{Q_H \times Q_O}{d_{OH}}$. According to Table 1, the bond strengths in the excited states are weaker than those in the ground states, while the $Q_H \times Q_O$ values are correspondingly larger. This trend indicates that the hydrogen bond changes can be mainly attributed to the difference in the oxygen–hydrogen distances. However, since the oxygen–hydrogen distances are dependent variables, the weakening of the hydrogen bonds are actually due to the molecular conformation changes resulting from the weaker double bonds. Once the molecular conformation changes, the polarized charges on the hydrogen and oxygen atoms will be increased to counter the change.

Table 1 Parameters included in the molecular vibration

	Y1-trimer-B	**Y2**-trimer-B	**Y3**-trimer-B
O_{34}	1.491	1.458	1.491
O'_{34}	1.371	1.350	1.394
$Q_3 + Q_4$	−0.1600	−0.1564	−0.2041
$Q'_3 + Q'_4$	−0.1798	−0.1685	−0.2171
$\frac{Q_5 \times Q_6}{d_{56}}$	−0.04520	−0.03598	−0.04768
$\frac{Q'_5 \times Q'_6}{d'_{56}}$	−0.04446	−0.03530	−0.04703
$Q_5 \times Q_6$	−0.09581	−0.07994	−0.1001
$Q'_5 \times Q'_6$	−0.09740	−0.08099	−0.1012

The analysis stated above provides more detailed information about the charge and conformation changes between the excited and ground states. In principle, the difference in these polymers in terms of their photothermal efficiency is a result of the total energy change. So, we further analyzed the relative energies of the molecules with different dihedral conformations. As shown in Fig. S26,† the dihedral angles corresponding to the points with zero relative energy follow the order of **Y3** < **Y1** < **Y2**, which is consistent with the previous calculation of S_0V_0. Increasing or decreasing the dihedral angle leads to a gradual increase in free energy, which indicates that the molecular distortion is restricted. However, since the hydrogen bond is a relatively weak bond and the double bond is weaker than that of ethylene, the rotation is not completely forbidden. There are more than 20 degrees below the gray dashed-dots for all of the polymers (Fig. S26†), indicating that the rotation is allowed within a certain range at room temperature. The high

photothermal efficiencies of these polymers can be mainly attributed to the flexible hydrogen bonding, which allows the excited molecules back to the ground state through the pathway of vibrational relaxation. Furthermore, the curves in Fig. S26† are differentiated by the dihedral angle. The slopes of the linear regions that cover θ and θ' in Fig. 5c represent the rate of relative energy change from S_1V_0 to S_0V_0, which can be used to evaluate the degree of difficulty of the molecular rotation. The slopes of **Y1**, **Y2**, and **Y3** are 0.00040, 0.00041, and 0.00036, respectively. The smaller slope of **Y3** represents easier molecular rotation along the 3–4 double bond at the same angle. In this regard, both the hydrogen and double bonds possess a certain flexibility in the excited state, which also provides preconditions and possibilities for the efficient photothermal conversion.

Conclusions

In conclusion, we have provided insights into three low bandgap polymers to understand the influence that intramolecular hydrogen bonding has on the light absorption and photothermal conversion properties. Following the rule of coupling molecular rigidity and flexibility, the three polymers all have remarkable absorption in the NIR-II window, and meanwhile possess excellent photothermal conversion capability. However, in view of the lack of theoretical research on the molecular design of NIR-II photothermal polymers and the scarcity of related studies on the structure–activity relationship, this work combines experiments with theoretical calculations to provide insights into the structure–property relationship and theoretical analysis of NIR-II photothermal molecular design, which is hoped to reinforce the photothermal knowledge relevant to conjugated polymers. Molecular structures in the ground and excited states were thoroughly analysed, and some new understanding in regard to the molecular structure has also been provided. Furthermore, the differences in the energy gap and dihedral angle are explained by the atomic conjugation effect and induction effect, which we believe will enlighten the design of functional photothermal polymers that exhibit higher light absorption and photothermal efficiency.

Conflicts of interest

There are no conflicts to declare.

Acknowledgements

This work was financially supported by the National Natural Science Foundation of China (22005336, 21875291, 21702240, and 21825503). Resources supporting this work were provided by the High-performance Computing Platform of Renmin University of China. The authors would like to thank Dr Ze-Fan Yao and Zhen Wang for their helpful discussion.

Notes and references

1 Y. Yang, P. He, Y. Wang, H. Bai, S. Wang, J.-F. Xu and X. Zhang, *Angew. Chem., Int. Ed.*, 2017, **56**, 16239–16242.
2 Y. He, Y. Cao and Y. Wang, *Asian J. Org. Chem.*, 2018, **7**, 2201–2212.
3 A. M. Smith, M. C. Mancini and S. Nie, *Nat. Nanotechnol.*, 2009, **4**, 710–711.
4 Y. Jiang, J. Li, X. Zhen, C. Xie and K. Pu, *Adv. Mater.*, 2018, **30**, 1705980.
5 B. Li, L. Lu, M. Zhao, Z. Lei and F. Zhang, *Angew. Chem., Int. Ed.*, 2018, **57**, 7483–7487.
6 G. Wen, X. Li, Y. Zhang, X. Han, X. Xu, C. Liu, K. W. Y. Chan, C.-S. Lee, C. Yin, L. Bian and L. Wang, *ACS Appl. Mater. Interfaces*, 2020, **12**, 33492–33499.
7 C. Yin, X. Li, G. Wen, B. Yang, Y. Zhang, X. Chen, P. Zhao, S. Li, R. Li, L. Wang, C.-S. Lee and L. Bian, *Biomaterials*, 2020, **232**, 119684.
8 Y. He and Y. Wang, *Acta Polym. Sin.*, 2019, **50**, 102–108.
9 Z. Cao, L. Feng, G. Zhang, J. Wang, S. Shen, D. Li and X. Yang, *Biomaterials*, 2018, **155**, 103–111.
10 T. Sun, J.-H. Dou, S. Liu, X. Wang, X. Zheng, Y. Wang, J. Pei and Z. Xie, *ACS Appl. Mater. Interfaces*, 2018, **10**, 7919–7926.
11 B. Guo, Z. Sheng, Kenry, D. Hu, X. Lin, S. Xu, C. Liu, H. Zheng and B. Liu, *Mater. Horiz.*, 2017, **4**, 1151–1156.
12 J. Wu, L. You, L. Lan, H. J. Lee, S. T. Chaudhry, R. Li, J.-X. Cheng and J. Mei, *Adv. Mater.*, 2017, **29**, 1703403.
13 H. Zhu, P. Cheng, P. Chen and K. Pu, *Biomater. Sci.*, 2018, **6**, 746–765.
14 Y. Cao, J.-H. Dou, N.-j. Zhao, S. Zhang, Y.-Q. Zheng, J.-P. Zhang, J.-Y. Wang, J. Pei and Y. Wang, *Chem. Mater.*, 2017, **29**, 718–725.
15 Y. Kai, X. Huan, C. Liang, S. Chunyang, W. Jun and L. Zhuang, *Adv. Mater.*, 2012, **24**, 5586–5592.
16 L. Li, Y. Liu, P. Hao, Z. Wang, L. Fu, Z. Ma and J. Zhou, *Biomaterials*, 2015, **41**, 132–140.
17 J. Li, J. Rao and K. Pu, *Biomaterials*, 2018, **155**, 217–235.
18 Y. Wang, W. Zhu, W. Du, X. Liu, X. Zhang, H. Dong and W. Hu, *Angew. Chem., Int. Ed.*, 2018, **57**, 3963–3967.
19 G. Qian and Z. Y. Wang, *Chem.–Asian J.*, 2010, **41**, 1006–1029.
20 Y. Cai, L. Huo, X. Sun, D. Wei, M. Tang and Y. Sun, *Adv. Energy Mater.*, 2015, **5**, 1500032.
21 Y. Lin and X. Zhan, *Adv. Energy Mater.*, 2015, **5**, 1501063.
22 L. Zhan, S. Li, H. Zhang, F. Gao, T.-K. Lau, X. Lu, D. Sun, P. Wang, M. Shi, C.-Z. Li and H. Chen, *Adv. Sci.*, 2018, **5**, 1800755.
23 Z. Yao, X. Liao, K. Gao, F. Lin, X. Xu, X. Shi, L. Zuo, F. Liu, Y. Chen and A. K. Y. Jen, *J. Am. Chem. Soc.*, 2018, **140**, 2054–2057.
24 X. Li, F. Fang, B. Sun, C. Yin, J. Tan, Y. Wan, J. Zhang, P. Sun, Q. Fan, P. Wang, S. Li and C.-S. Lee, *Nanoscale Horiz.*, 2021, **6**, 177–185.
25 A. Onwubiko, W. Yue, C. Jellett, M. Xiao, H.-Y. Chen, M. K. Ravva, D. A. Hanifi, A.-C. Knall, B. Purushothaman, M. Nikolka, J.-C. Flores, A. Salleo, J.-L. Bredas, H. Sirringhaus, P. Hayoz and I. McCulloch, *Nat. Commun.*, 2018, **9**, 416.
26 N. M. Randell, P. C. Boutin and T. L. Kelly, *J. Mater. Chem. A*, 2016, **4**, 6940–6945.
27 T. Lei, J.-H. Dou, X.-Y. Cao, J.-Y. Wang and J. Pei, *J. Am. Chem. Soc.*, 2013, **135**, 12168–12171.

28 Y. He, J. Quinn, Y. Deng and Y. Li, *Org. Electron.*, 2016, **35**, 41–46.
29 E. A. Castro, *Chem. Rev.*, 1999, **99**, 3505–3524.
30 E. Wang, W. Mammo and M. R. Andersson, *Adv. Mater.*, 2014, **26**, 1801–1826.
31 M. Kasha, *Radiat. Res.*, 1963, **20**, 55–70.
32 K. Cai, J. Xie, D. Zhang, W. Shi, Q. Yan and D. Zhao, *J. Am. Chem. Soc.*, 2018, **140**, 5764–5773.
33 N. J. Turro, V. Ramamurthy and J. C. Scaiano, *Modern Molecular Photochemistry of Organic Molecules*, University Science Books, Mill Valley, California, 2009.
34 Y. Lu, Z. D. Yu, R. Z. Zhang, Z. F. Yao, H. Y. You, L. Jiang, H. I. Un, B. W. Dong, M. Xiong, J. Y. Wang and J. Pei, *Angew. Chem., Int. Ed.*, 2019, **58**, 11390–11394.
35 T. Lu and F. Chen, *J. Comput. Chem.*, 2012, **33**, 580–592.
36 P. M. Beaujuge, C. M. Amb and J. R. Reynolds, *Acc. Chem. Res.*, 2010, **43**, 1396–1407.
37 T. Lu and F. Chen, *J. Phys. Chem. A*, 2013, **117**, 3100–3108.
38 T. Steiner, *Angew. Chem., Int. Ed.*, 2002, **41**, 48–76.